Supplementary information

Stimuli-free Zn/soda-lime glass/CuO based MIS device for sensing human skin moisture

*Kanhai Kumar, [a‡] Hemam Rachna Devi, [a‡] Gokul Raj, [a] and Karuna Kar Nanda [a,b,c,]**

[a]Materials Research Centre, Indian Institute of Science, Bangalore-560012, India

[b]Institute of Physics, P. O. Sainik School, Bhubaneswar – 751005, India

[c]Homi Bhabha National Institute, Mumbai, Maharashtra – 400094, India

KEYWORDS: Proximity sensor, interdigitated, soda-lime glass, humidity sensing

Entry for the Table of Contents
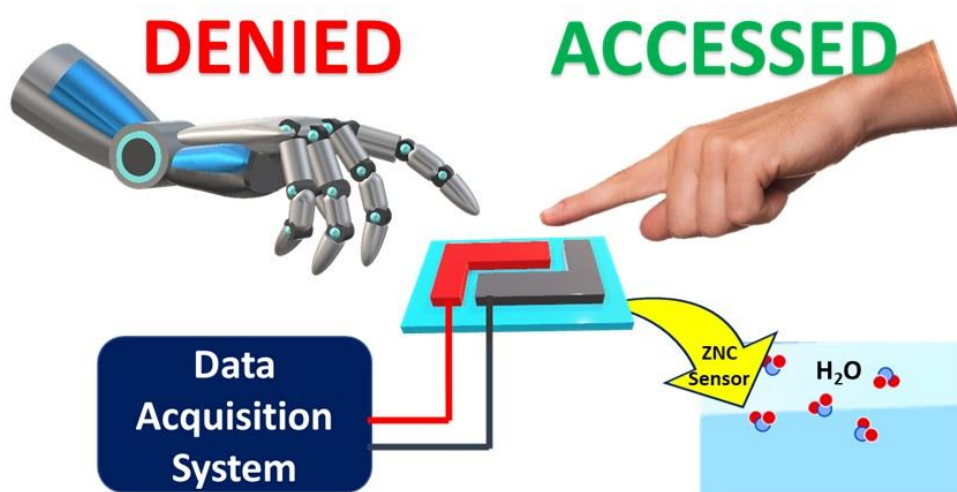
1. FILM DEPOSITION CONDITIONS

Devices based on the interdigitated pattern of Zn and CuO thin films (denoted as ZNC) on SLG are fabricated by sputtering. Prior to the deposition of the films, the substrate is washed thoroughly with ethanol (99.9% purity) and dried in a vacuum oven at 80 °C. At first, the Cu thin film is sputtered using the Cu target (3-inch target procured from Kurt J. Lesker) onto the SLG. Subsequently, the sample is annealed at 600 °C for 3 h to obtain CuO. Further, CuO thin film is masked, and Zn is sputtered to get the interdigitated pattern. The detail of the sputtering conditions for ZNC is presented in Table S1.

Table S1. Parameters for deposition of Cu and Zn films using DC sputtering.

Target	Deposition time (min)	DC power (Watt)	Working pressure (10^{-3}mbar)	Deposition temperature (°C)
Copper	15	50	8.4	RT
Zinc	15	35	8.4	RT

The individual Zn and CuO thin films were characterized by X-Ray diffraction (XRD). The XRD data were gathered at room temperature with 2Ө scan range between 5 to 90° using a wide-angle X-ray diffractometer (PANalytical) equipped with a Cu Kα radiation (1.54 Å). Raman spectra are recorded using WITec system with a 532 nm excitation wavelength. The morphological characterizations were performed using Scanning Electron Microscopy (SEM) using FESEM FEI inspect 5.0. X-Ray photoelectron. X-ray photoelectron spectroscopy (XPS) measurements were performed in AXIS ULTRA DLD Kratos possessing a monochromatic Al

Kα radiation source of 1486.6 eV. Atomic force microscopy images were obtained using A.P.E

Research, Model A-100.

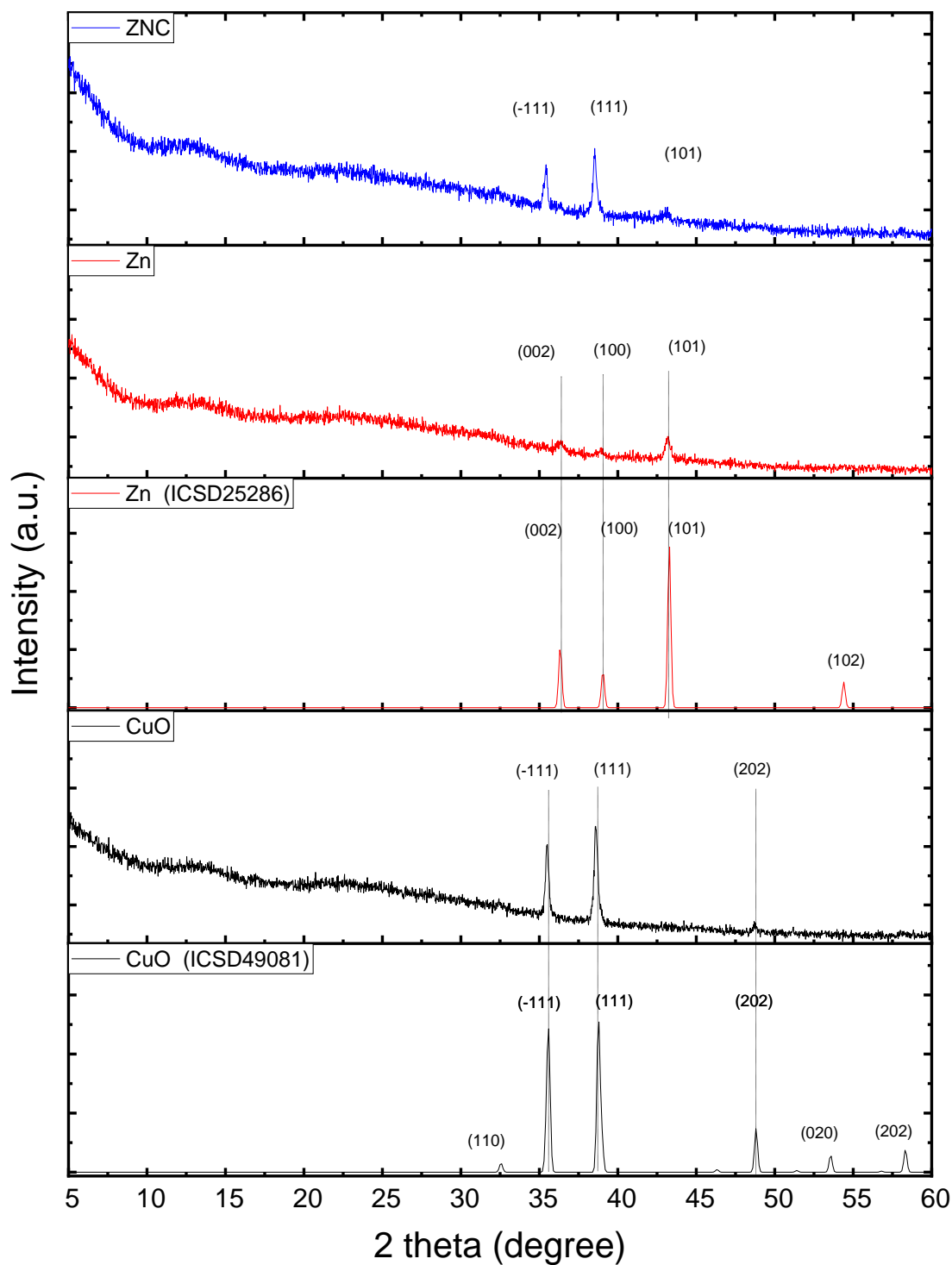2. X-RAY DIFFRACTION ANALYSIS - WIDE SCAN

Figure S1. Wide scan of X-ray diffraction of CuO, Zn and ZNC sensor.
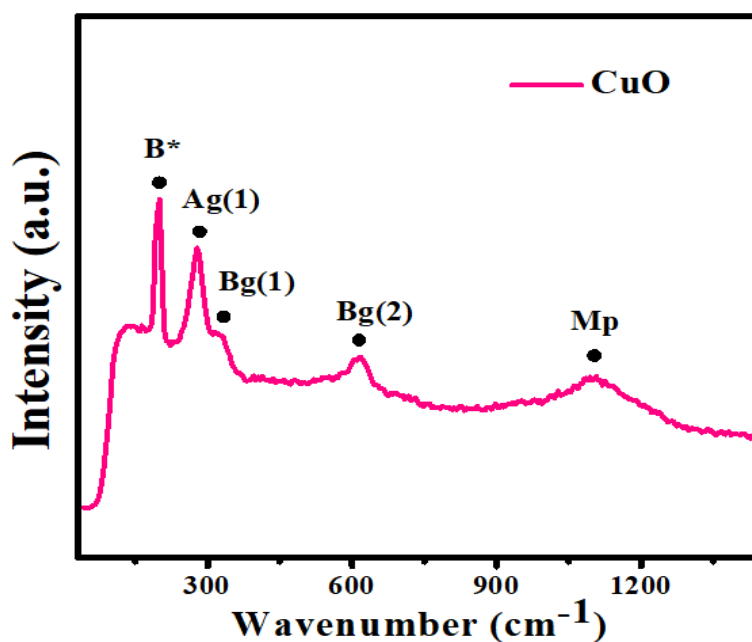
3. RAMAN ANALYSIS

Figure S2. Raman spectrum of CuO in ZNC sensor.

4. GOLD PLATING AND SEM ELEMENTAL SPECTRUM

4.1. Procedure for gold plating

Consciously, for better Scanning electron microscopic images, we have performed for 2 min the gold plating using the sputtering method using the JOEL Smart coater with the resulting 5nm/min thickness.

4.2. SEM-EDS elemental spectrum

In both cases of thin films, a wide area is selected and scanned with Zeiss Gemini ULTRA 55 scanning electron microscopy.

4.3. SEM-EDS spectrum

As, Figure S3 and S4 shows the presence of various elements as well as the elements of our interest. Literature have admitted these expected elemental presence and can be found elsewhere.[1,2]
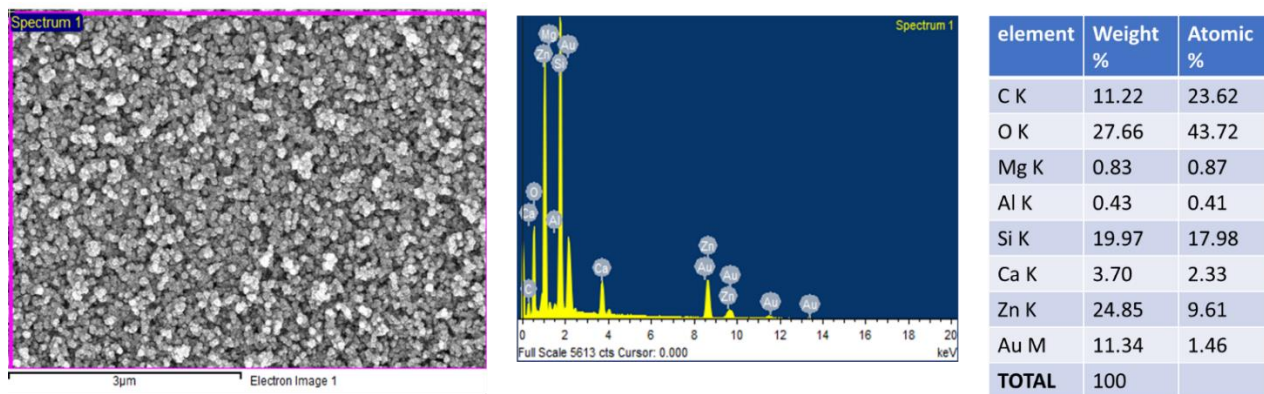
element	Weight %	Atomic %
C K	11.22	23.62
O K	27.66	43.72
Mg K	0.83	0.87
Al K	0.43	0.41
Si K	19.97	17.98
Ca K	3.70	2.33
Zn K	24.85	9.61
Au M	11.34	1.46
TOTAL	100	

Figure S3. Area SEM-EDS spectrum and the atomic and weight percentage of various elements of Zn thin films.

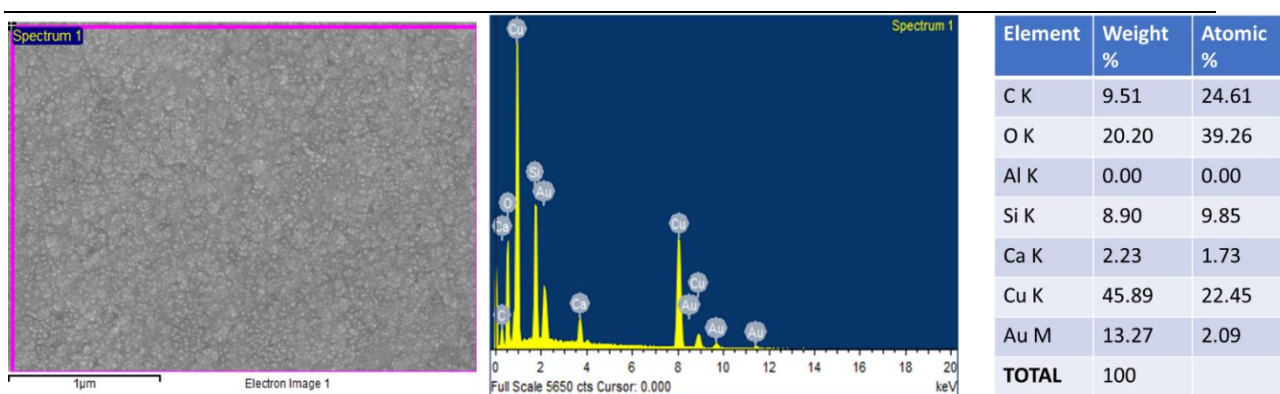| Element	Weight %	Atomic %
C K	9.51	24.61
O K	20.20	39.26
Al K	0.00	0.00
Si K	8.90	9.85
Ca K	2.23	1.73
Cu K	45.89	22.45
Au M	13.27	2.09
TOTAL	100	

Figure S4. Area SEM-EDS spectrum and the atomic and weight percentage of various elements for CuO thin films.

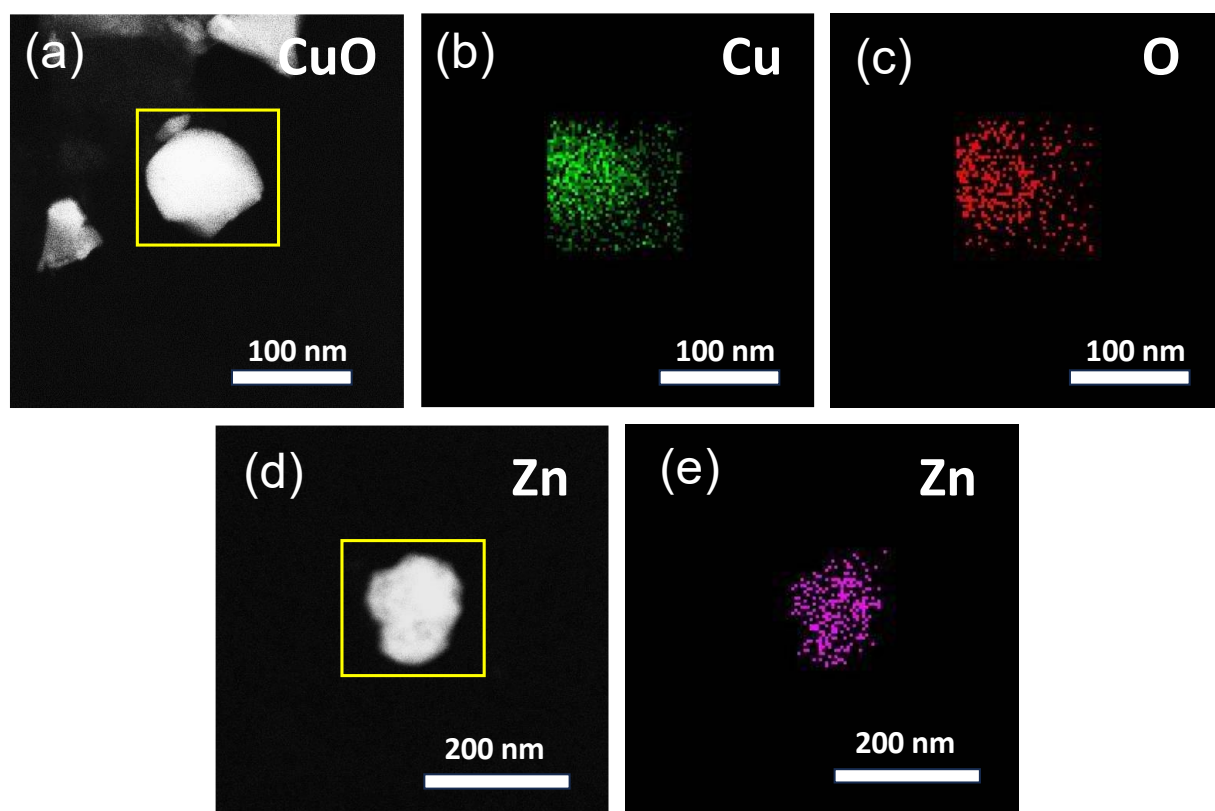## 5. TRANSMISSION ELECTRON MICROSCOPY ANALYSIS

Figure S5. Transmission electron microscopic images with elemental mapping with an intention to represent the elemental distribution of CuO (a-c) and Zn (d-e) respectively.

6. MOTT-SCHOTTKY ANALYSIS

Mott-Schottky measurement was performed in CHI electrochemical workstation with varying potentials in the range of 1 to -0.8V vs Ag/AgCl at a fixed frequency of 1KHz in a 1M KOH medium in order to extricate the carrier type and carrier density of CuO.

Equation S1: Mott-Schottky equation

$$\frac{1}{C^2} = \frac{2}{\epsilon\epsilon_0 \, eA^2 \, N_A} \left(V - V_F - \frac{KT}{e}\right)$$

where C = differential capacitance of the space charge region, ϵ = dielectric constant, $\epsilon 0$ = vacuum permittivity, e = charge of the electron, A = surface area of the electrode, N_A = acceptor density, V = applied potential, V_F = flat-band potential, K = Boltzmann constant, T = Temperature.

7. SENSITIVITY CALCULATION:

Equation S2. Sensitivity calculation

$$S = \frac{(R_g - R_a)}{R_a} \times 100\%$$

Where, S, R_g, and R_a are sensitivity, resistance in moisture and resistance in air respectively.

Sensitivity (S (%)) is come out to be 11330.8.[3]
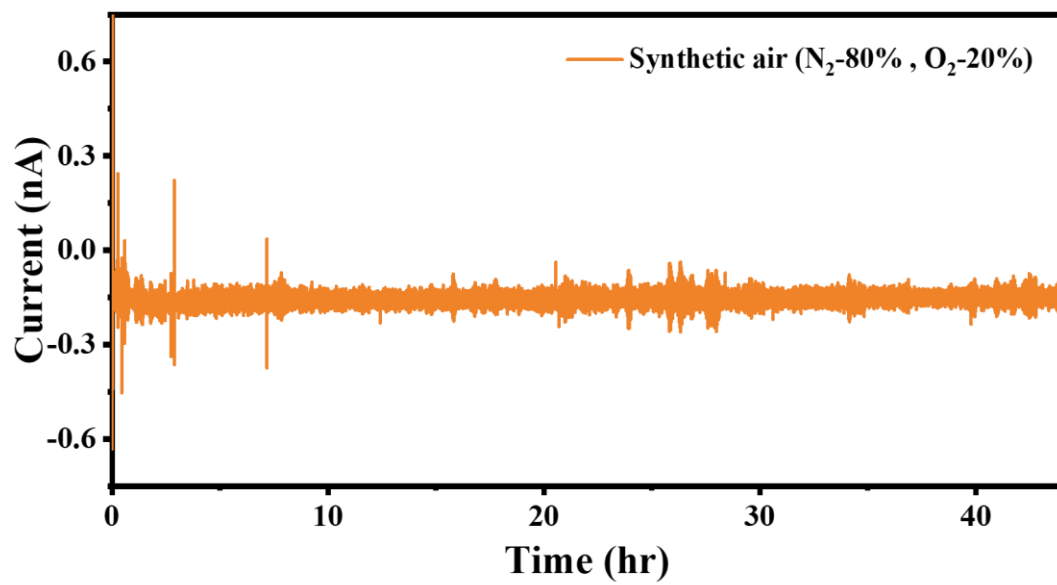
8. STABILITY PERFORMANCE

Figure S6. Stability performance for ZNC sensor in synthetic air environment.
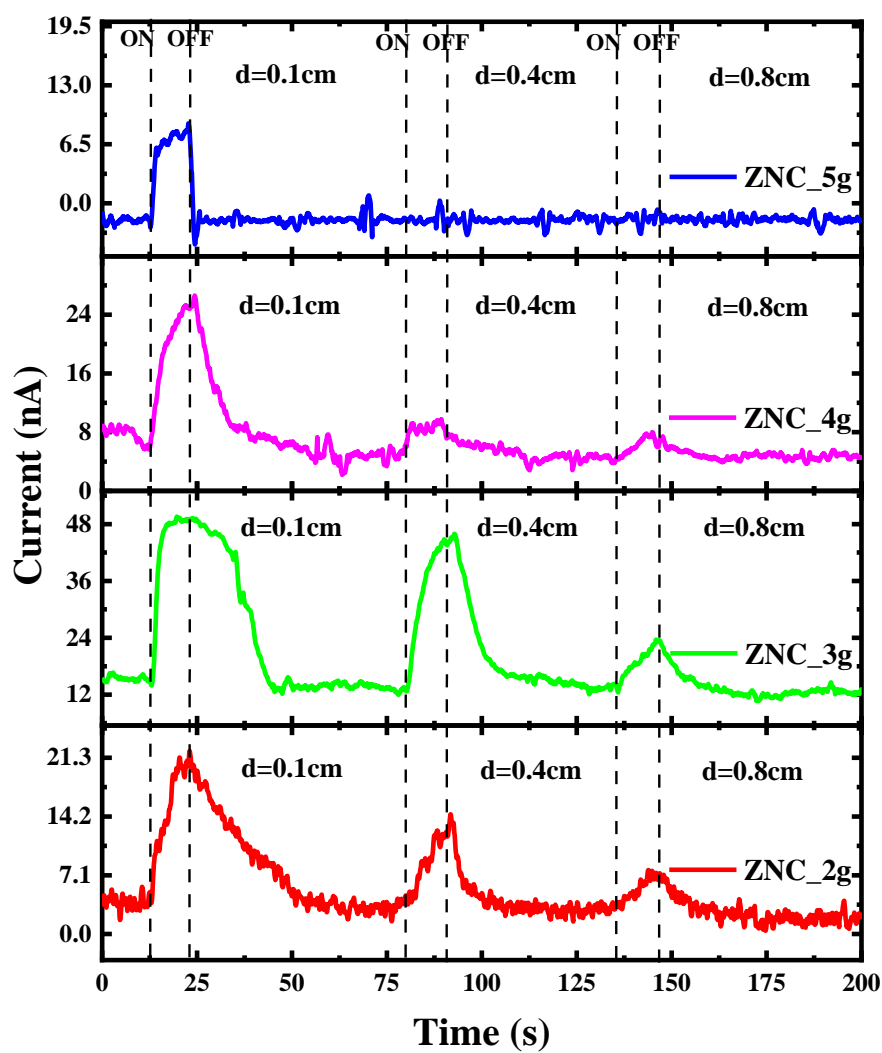
9. IN-BUILT CURRENT GENERATION

Figure S7. Current response of ZNC_2g, ZNC _3g, ZNC _4g and ZNC _5g in the proximity of human finger w.r.t distance (cm).
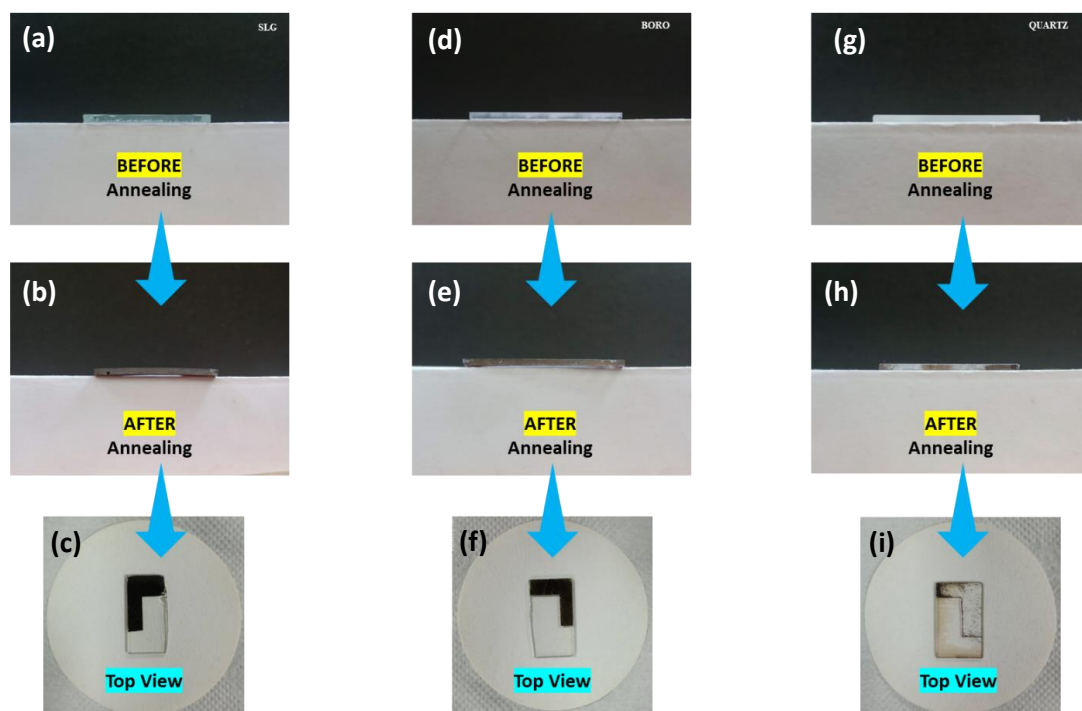
10. THERMAL EFFECT ANALYSIS

Figure S8. Photograph of CuO on (a,b,c) SLG, (d,e,f) borosilicate, and (g,h,i) quartz before and after annealing at 600 °C.
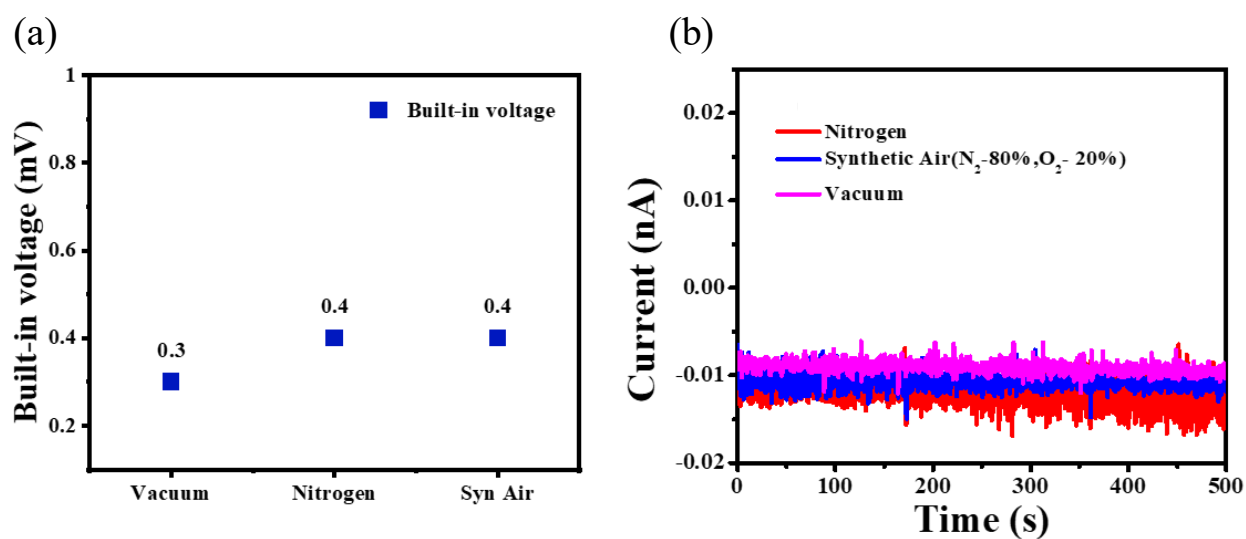
11. IONIC EFFECT ANALYSIS

Figure S9. (a) In-built voltage and, (b) current of ZNC device at different environmental conditions.

12. CORRELATIONS OF RESPONSE ARISES

Equation S3: Exponential expression

$$V_{in} = K e^{-\frac{d}{d_0}}$$

Equation S4: Natural logarithmic expression

$$\ln(V_{in}) = \ln(K) - {d}/{Ad_0}$$

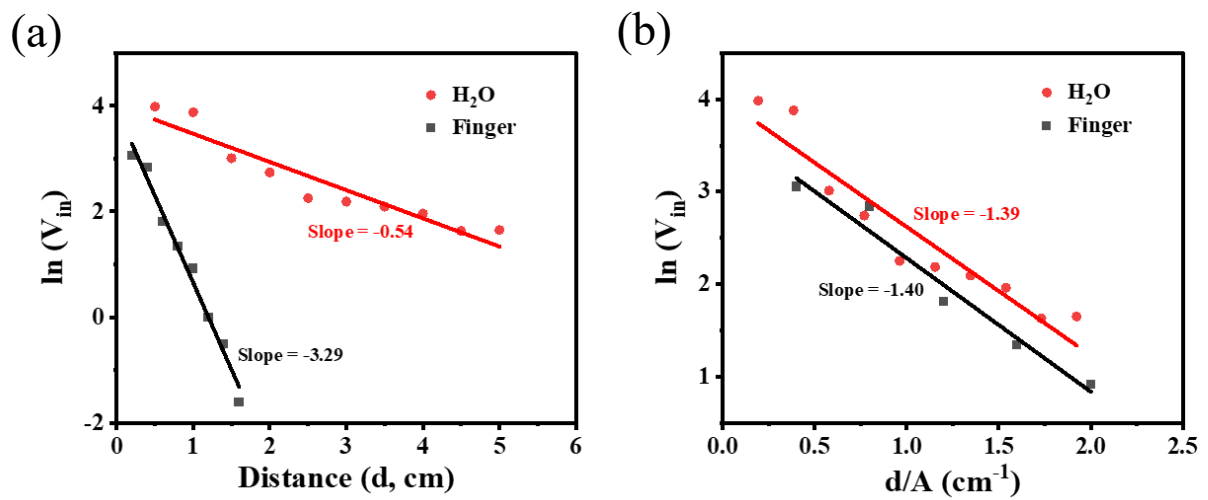12.1. Natural logarithmic relations of finger and water.

Figure. S10. Natural logarithmic relations of (a) finger and water, and (b) distance normalized w.r.t exposed area.

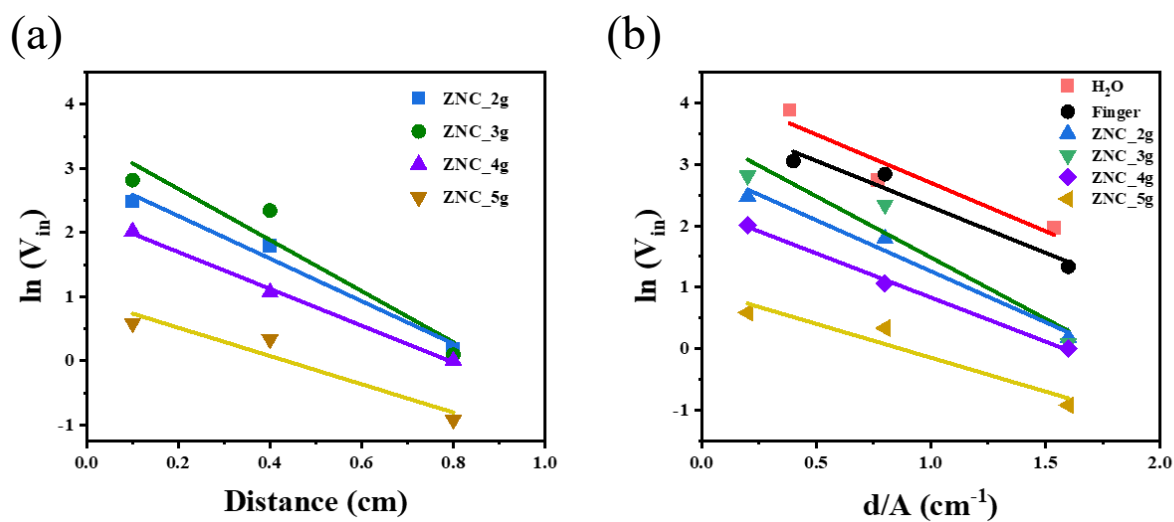12.2. Relations with different sensors and its comparison with finger and water observations

Figure. S11. Natural logarithmic with normalized w.r.t exposed area relations of (a) different

sensors, and (b) comparison with finger and water observations.
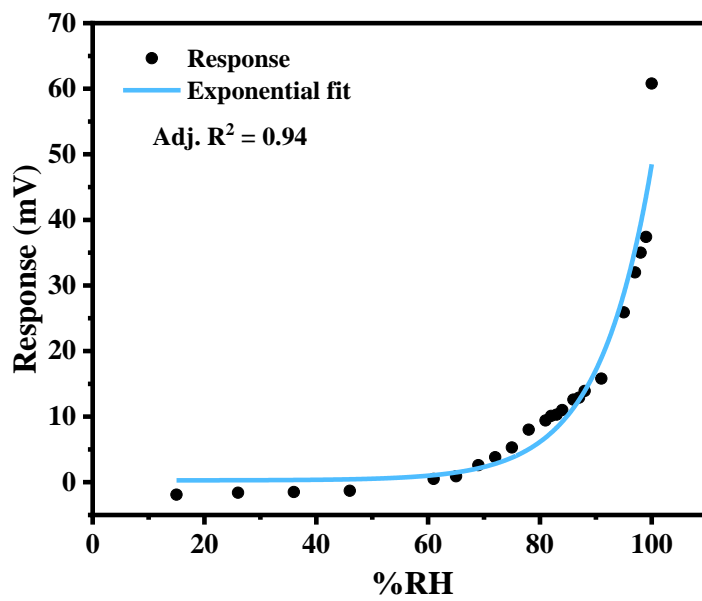
13. RESPONSE VS %RH ANALYSIS

Figure. S12. Humidity Measurement in Vacuum Chamber

TABLE OF COMPARISON

Table S2. Comparison of our ZN/CuO device with other reported literature

Materials	Method(s)	Sensitivity & at %RH	Temp	Response (s)	Recovery (s)	References
CuO nanostructures	Hydrothermal	- 30-90%RH	RT	126	20	[a][4]
ZnO nanoparticles	Wire electrical explosion method	- 11-95%RH	25°C	40	50	[b][5]
ZnO/CuO nanocomposite	Microwave synthesis	5.3 15-95%RH	600°C	158	426	[c][6]
CuO-ZnO nanostructures	Nebulized assisted spray pyrolysis method	2.33 at MΩ/%RH 25-90 %RH	RT	29	16	[d][7]
CuO Mesoporous particles	Thermal decomposition	- 33-90%RH	RT	1	1	[e][8]
CuO Nanoparticles	Thermal annealing	- 20-80% RH	25°C	98	98	[f][9]
CuO Nanosheets	hydrothermal	11.3-97.3%RH	25°C	32	22	[g][10]

CuO Nanofilm	SILAR	- 20-80% RH	25°C	130	320	[h][11]
CuO nanosheets	Spin-spray method	170% 20–90% RH	RT	2.1 s	2.8 s	[i][12]
GO/MWCNT	Modified Hummers method	7980% 11–97%RH	25°C	5 s	2.5 s	[j][13]
MWCNT/Nafion nanofibers film	Electrospinning method	427.6% 10–80%RH	23 ±1.5°C	3 s	-	[k][14]
PEO−CuO−MWCNT: 1%	Precipitation and electrospinning method	3798.2% 30–90%RH	RT	3s	22s	[l][15]
PEO−CuO−MWCNT: 3%	Precipitation and electrospinning method	53837.6% 30-90%RH	RT	20s	11 s	[m][15]
Zn/CuO	**DC sputtering**	**11330.8%** -	**RT**	**~1.8s**	**~1.9s**	**This work**

14. ILLUSTRATIVE OBSERVATIONS OF DIFFERENT INANIMATE OBJECTS

We performed the experiments using different inanimate objects i.e., Gloves, Robot/Toy, writing marker/pen, Tissue paper, goggles with finger which can found in S13 with media as **SIM1**.
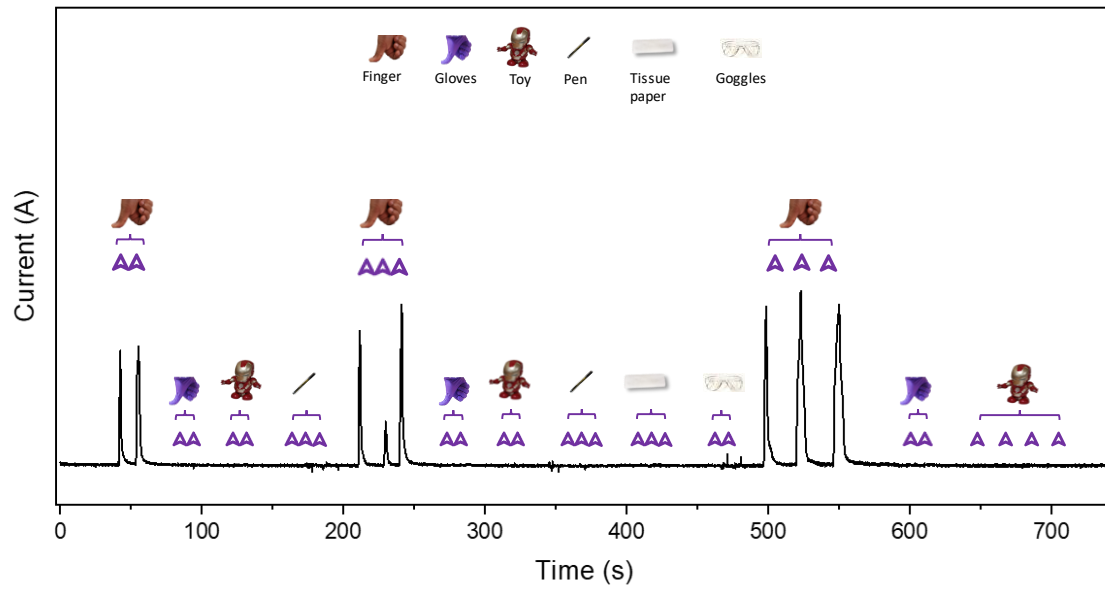

Figure. S13. Illustration of response generated from different inanimate objects including finger.

REFERENCES:

1   Riyatun, P. L. Bintari, H. Purwanto and A. Marzuki, *J. Phys. Conf. Ser.*, 2019, **1153,** 012084.

2   K. V. Sopiha, J. H. Kim, S. S. Kim and P. Wu, *Sensors Actuators, B Chem.*, 2018, **266**, 344–353.

3   Y. Li, H. Ban and M. Yang, *Sensors Actuators, B Chem.*, 2016, **224**, 449–457.

4   J. Wang and W. Zeng, *J. Sensors*, 2022, **2022**, 7749890

5   Q. Qi, T. Zhang, Y. Zeng and H. Yang, *Sensors Actuators, B Chem.*, 2009, **137**, 21–26.

6   C. Ashok, K. V. Rao and C. S. Chakra, *Chem. Sci. J. Adv. Chem. Sci.*, 2016, **2**, 223–226.

7   A. S. Pathan, D. L. Gapale, S. V. Bhosale, A. S. Landge, S. R. Jadkar and S. A. Arote, *Inorg. Chem. Commun.*, 2023, **153**, 110824.

8   K. Malook, H. Khan, M. Ali and Ihsan-Ul-Haque, *Mater. Sci. Semicond. Process.*, 2020, **113**, 105021.

9   S. B. Wang, C. H. Hsiao, S. J. Chang, K. T. Lam, K. H. Wen, S. J. Young, S. C. Hung and B. R. Huang, *IEEE Sens. J.*, 2012, **12**, 1884–1888.

10   Y. Gu, H. Jiang, Z. Ye, N. Sun, X. Kuang, W. Liu, G. Li, X. Song, L. Zhang, W. Bai and X. Tang, *Electron. Mater. Lett.*, 2020, **16**, 61–71.

11   P. M. Perillo and D. F. Rodriguez, in *Anales Afa*, 2021, **32**, 76–82.

12   R. Nitta, H. E. Lin, Y. Kubota, T. Kishi, T. Yano and N. Matsushita, *Appl. Surf. Sci.*, 2022, **572**, 151352.

13   X. Li, X. Chen, X. Chen, X. Ding and X. Zhao, *Mater. Chem. Phys.*, 2018, **207**, 135–140.

14   L. Sheng, C. Dajing and C. Yuquan, *Nanotechnology*, 2011, **22,** 265504.

15   W. Ahmad, B. Jabbar, I. Ahmad, B. M. Jan, M. M. Stylianakis, G. Kenanakis and R. Ikram, *Materials (Basel).*, 2021, **14**, 1–19.